Available online at www.sciencedirect.com
SCIENCE DIRECT
Chemical Physics 326 (2006) 589–599
Chemical Physics
www.elsevier.com/locate/chemphys

Ionic fragmentation of C 1s excited and ionized formic acid

A.C.O. Guerra [a,b], J.B. Maciel [b], C.C. Turci [b], H. Ikeura-Sekiguchi [c], A.P. Hitchcock [a,*]

[a] Department of Chemistry, McMaster University, Hamilton, ON, Canada L8S 4M1
[b] Instituto de Química, Universidade Federal do Rio de Janeiro, Rio de Janeiro, RJ 21949-900, Brazil
[c] National Institute of Advanced Industrial Science and Technology, Tsukuba, Ibaraki 305-8568, Japan

Received 11 January 2006; accepted 13 March 2006
Available online 21 April 2006

Abstract

Time of flight mass spectrometry with multi-ion coincidence detection has been used to investigate ionic photofragmentation of four isotopes of gaseous formic acid [HCOOH, HCOOD, DCOOH and DCOOD] following C 1s excitation and ionization. C 1s spectra, branching ratios and quantitative yields of ions and ion pairs are reported. For equivalent ionic decay channels in the four isotopes the partial ion and ion pair yield spectra are very similar. These gas phase results are compared to results from photon stimulated ion desorption (PSID) of deuterated formate adsorbed on Si(100) [H. Ikeura-Sekiguchi, T. Sekiguchi, K. Tanaka, Phys. Rev. B 53 (1996) 12655] where there is a very strong enhancement of the D^+ yield at C 1s $\rightarrow \sigma^*_{C-D}$ resonance and the COD^+ yield at the C 1s $\rightarrow \sigma^*_{C-O}$ resonance. Such enhancements were not observed in the fragmentation of gas phase formic acid. From this we conclude that these very specific bond breaking processes in surface adsorbed formate are associated with a minority channel such as a (2*h*, 1*e*) spectator Auger process, which becomes prominent through elimination of the dominant molecular fragmentation mechanisms by electronic recombination.

Keywords: Formic acid; Isotopes; Time-of-flight mass spectrometry; Inner-shell excitation; Cross-sections; Photofragmentation; PEPICO; PIPICO; PEPIPICO; Partial ion yield; Branching ratio

1. Introduction

The binding of organic molecules to silicon surfaces and their subsequent interactions with radiation are of considerable interest, due to diverse applications such as molecular electronics, biosensors, nonlinear optics, etc. Formic acid is the simplest carboxylic acid and serves as a model for other organic acids with more complicated chemical structures [1]. On most metal and semiconductor surfaces including silicon, carboxylic acids adsorb dissociatively to form bound carboxylate species [2] and thus DCOOH binds to Si as the formate ion ($DCOO^-$). In 1996, Ikeura-Sekiguchi et al. [3] reported measurements of photon stimulated ion desorption (PSID) from a monolayer of deutero-formate chemisorbed on Si(100). They reported partial ion yield spectra for the four dominant ions – D^+, CDO^+, O^+ and CD^+. These spectra exhibited C 1s spectral features which reflected the local bonding character of the electronic states involved. In particular the D^+ yield was very enhanced at the C 1s $\rightarrow \sigma^*_{C-D}$ transition (292 eV) and the CDO^+ yield was enhanced at the C 1s $\rightarrow \sigma^*_{C-O}$ transition (298 eV), suggesting that bond specific fragmentation was occurring, perhaps through an ultrafast decay process in which bond breaking occurs before core hole decay [4,5]. These results were in strong contrast to many other results for monolayer adsorbates on metals and semiconductors [6–9] where the partial yields of fragment ions typically only appear far in the continuum since multiple ionization shake-off processes are required to surmount the strong tendency for reneutralization and either neutral production or recombination of neutralized parent or fragment ions with the surface. *What is so special about*

* Corresponding author. Tel.: +1 905 525 9140x24749; fax: +1 905 521 2773.
E-mail address: aph@mcmaster.ca (A.P. Hitchcock).

0301-0104/$ - see front matter © 2006 Elsevier B.V. All rights reserved.
doi:10.1016/j.chemphys.2006.03.044

the formate/Si(100) case? Could there be intrinsic molecular processes such as ultrafast dissociation that drive the observed PSID [3]? In order to investigate this possibility, we have examined the ionic photofragmentation of C 1s excited and ionized formic acid in the gas phase. While it would be preferable to study the free formate species, this would require the capability to form a molecular beam of formate radicals or formate negative ions. Experiments on inner-shell photofragmentation of negative molecular ions (e.g. B_2^-, B_3^-, Ni_x^-) have been reported recently [10] but the technique was not accessible to us.

Inner-shell excitation and associated spectroscopies of ionic fragmentation of inner-shell states are site specific probes of electronic and geometrical structure and photoionization dynamics [5,11]. The combination of tunable synchrotron radiation and multi-ion coincidence time-of-flight mass spectrometry enables studies of the excitation and ionic fragmentation of inner-shell excited and ionized molecules. Auger decay of these states is an efficient source of multiply charged ions. The charge separation and fragmentation of those species can be studied by photoelectron–photoion coincidence (PEPICO), photoion–photoion coincidence (PIPICO) and photoelectron–photoion–photoion coincidence (PEPIPICO) techniques. Relative to examining individual time-of-flight mass spectra, partial ion yield (PIY) and partial ion pair yield (PIPY) spectroscopies can provide additional insights into ionic fragmentation through increased spectroscopic selectivity [12]. PIY and PIPY spectra, typically derived from branching ratios extracted from TOF mass spectra recorded at a sequence of photon energies, give a broad overview of the fragmentation of each state while multi-ion coincidence techniques

Table 1
Energies, term values, and proposed assignments for features observed in the C 1s total ion yield spectrum of formic acid

#	$E(\pm 0.1$ eV)	TV[a]	Assignment
1	288.2	7.6	π^*(C=O)
2	291.8	4.0	3s/σ^*(HCO/DCO)
3	293.2	2.6	3p
4 (sh)	294.2	1.6	Higher Rydberg
IP[b]	295.8		
5	297.1(3)	−1.3	σ^*(C–OH/C–OD)
6	303(1)	−7	σ^*(C=O)

[a] TV = IP–E.
[b] Ref. [31].

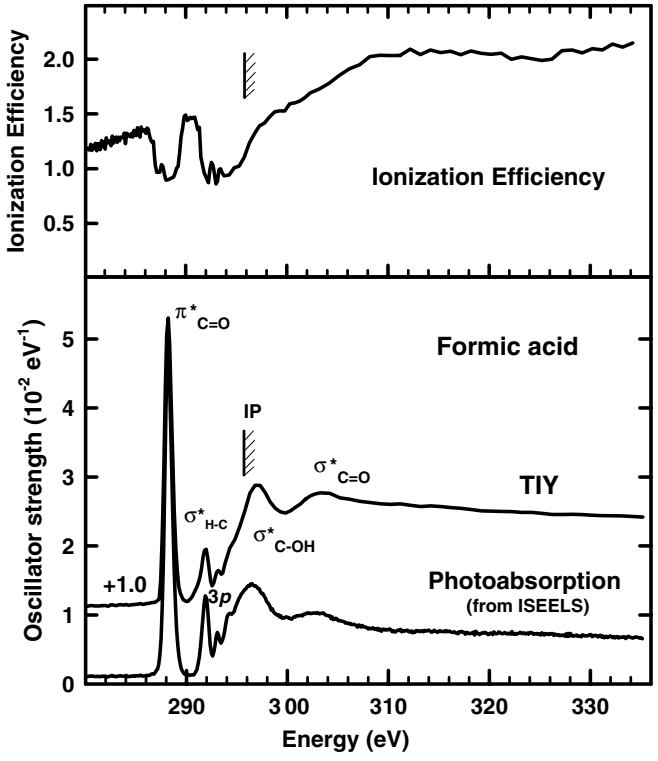

Fig. 1. Comparison of photoabsorption (derived from ISEELS [26]) and TIY spectra of HCOOH in the C 1s region. The top panel shows the ionization efficiency, derived as described in the text.

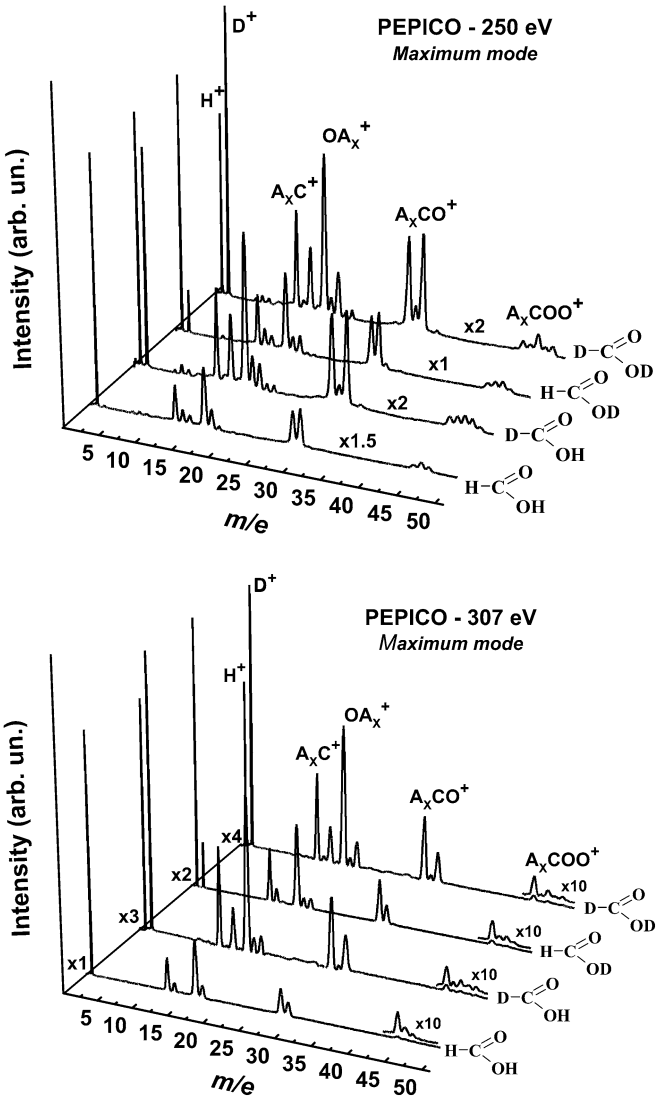

Fig. 2. Photoelectron–photoion coincidence (PEPICO) spectra for HCOOH, HCOOD, DCOOH and DCOOD, acquired in *maximum* ion mode at 250 eV (below any core level excitation) and at 307 eV, in the C 1s continuum. A = H or D.

help identify in more detail the fragmentation mechanisms involved.

In this study we have used a recently modified [13] Wiley–McLaren [14] time-of-flight mass spectrometer (TOF-MS) which incorporates an additional ion-focussing lens [15,16] to improve its quantitative performance. Multi-ion coincidence signals (PEPICO, PIPICO and PEPIPICO) have been used to study the ionic fragmentation following C 1s excitation and ionization of the four isotopes of formic acid (HCOOH, DCOOH, HCOOD and DCOOD). Other closely related studies include: NEXAFS, photoemission and ionic desorption studies of surface-adsorbed formate [3,17–24]; NEXAFS and fragmentation studies of gaseous and condensed methyl formate [25]; and gas phase studies of formic acid by inner-shell electron energy loss spectroscopy [26], valence shell photoionization [27] and gas phase photo-fragmentation dynamics [28,29]. We discuss our results in the context of these studies.

Table 2
Assignments for PEPICO signals based on flight time and mass-to-charge ratio (m/e)

m/e	Fragment
1	H^+
2	D^+
12	C^+
13	HC^+
14	DC^+/CO^{++}
16	O^+
17	OH^+
18	OD^+/H_2O^+
28	CO^+
29	HCO^+
30	DCO^+
44	COO^+
45	$HCOO^+$
46	$DCOO^+$
47	$DCOOH^+$
48	$DCOOD^+$

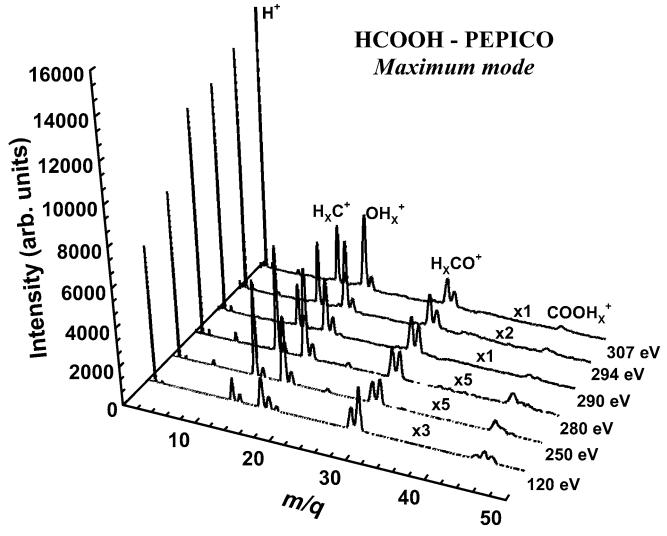

Fig. 3. PEPICO spectra for HCOOH, acquired in *maximum* ion mode at 120, 250, 280, 290, 294, and 307 eV.

2. Experimental

The experiments were performed using the Mark II grasshopper at the Synchrotron Radiation Center (SRC, University of Wisconsin at Madison). This monochromator, which is equipped with a 1200 lines/mm grating, provides about 10^9 photons per second in a 2×1 mm spot with a resolving power ($\Delta E/E$) of about 500. For the C 1s measurements a 100 nm thin film of Ti was placed in

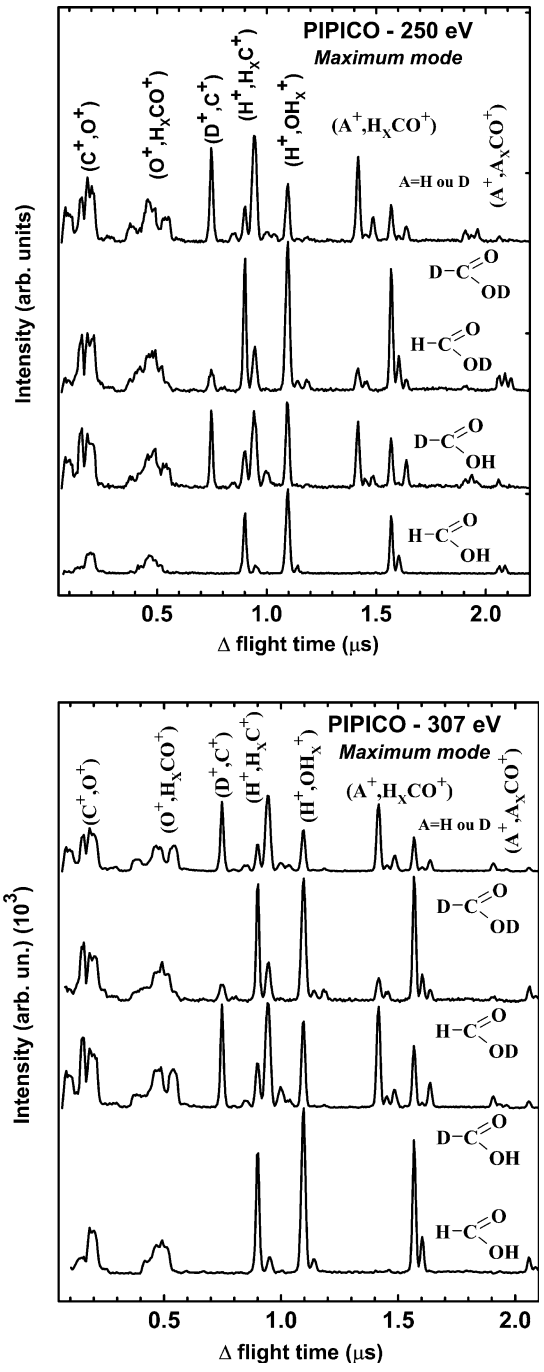

Fig. 4. Photoion–photoion coincidence (PIPICO) spectra for HCOOH, HCOOD, DCOOH and DCOOD, acquired in *maximum* ion mode at 250 eV.

the beam path, which reduced the second order radiation by 70%. Even so, second order and stray light signals are present at levels that are both difficult to estimate and which change across the C 1s photon energy range due to the effects of carbonaceous optics contamination.

Table 3
Assignments for PIPICO signals based on their difference flight time (Δt)

Δt-observed (μs)	Δt-predicted (μs)	Ion pair
0.09	0.09	$(CD^+,O^+)/(O^+,OD^+)$
0.15	0.15	(H^+,D^+)
0.19	0.19	$(C^+,O^+)/(CD^+,OD^+)$
0.42	0.41	(OD^+,HCO^+)
0.47	0.47	(O^+,CO^+)
0.52	0.51	$(O^+,HCO^+)/(O^+,DCO^+)$
0.75	0.74	(D^+,C^+)
0.85	0.84	(D^+,CD^+)
0.90	0.89	(H^+,C^+)
0.95	0.94	$(H^+,HC^+)/(D^+,O^+)$
1.00	1.00	$(H^+,CD^+)/(H^+,CO^{++})$
1.03	1.02	(D^+,OD^+)
1.10	1.08	$(H^+,O^+)/(H^+,CD^+)$
1.14	1.14	(H^+,OH^+)
1.19	1.17	(H^+,OD^+)
1.42	1.40	(D^+,CO^+)
1.45	1.44	(D^+,HCO^+)
1.49	1.48	(D^+,DCO^+)
1.57	1.56	(H^+,CO^+)
1.60	1.59	(H^+,HCO^+)
1.64	1.63	(H^+,DCO^+)
1.91	1.89	(D^+,COO^+)
1.94	1.92	$(D^+,HCOO^+)$
1.96	1.94	$(D^+,COOD^+)$
2.06	2.04	(H^+,COO^+)
2.09	2.07	$(H^+,HCOO^+)$
2.12	2.10	$(H^+,COOD^+)$

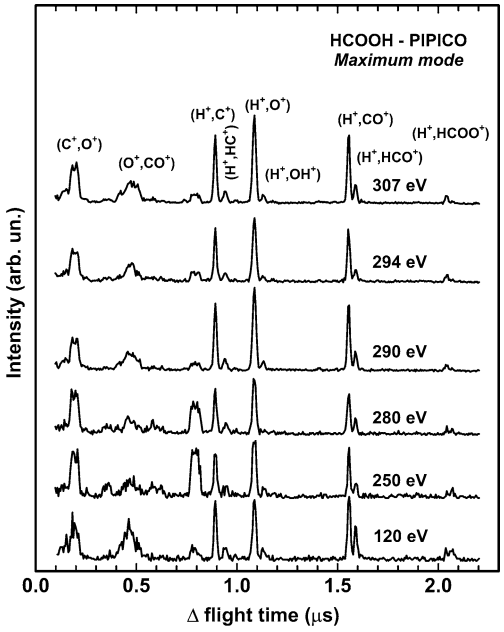

Fig. 5. PIPICO spectra for HCOOH, acquired in *maximum* ion mode at 120, 250, 280, 290, 294, and 307 eV.

The isotopically substituted formic acids were obtained commercially from Sigma–Aldrich (HCOOH ⩾ 96%; HCOOD – 95 wt. % in deuterium oxide, 98 atom % D; DCOOH – 95 wt. % in water, 98 atom % D; DCOOD – approximately 90 atom % D at the hydroxy position; 98 atom % D) and purified by removing air and volatile impurities by a series of freeze–pump–thaw cycles. The vapour above the liquid at room temperature was introduced into the ionization region of the time-of-flight apparatus through a leak valve. The sample pressure in the ionization region was maintained at $\sim 3 \times 10^{-6}$ torr during data acquisition. A low sample pressure was used in order to optimize the signal rate while keeping false coincidences to a minimum. The base pressure of the apparatus is $\sim 2 \times 10^{-8}$ torr without baking and $\sim 3 \times 10^{-9}$ torr after a mild bake. Unfortunately the sample inlet system was not conditioned prior to introducing species with a labile OD group and thus the data for the HCOOD and DCOOD samples are

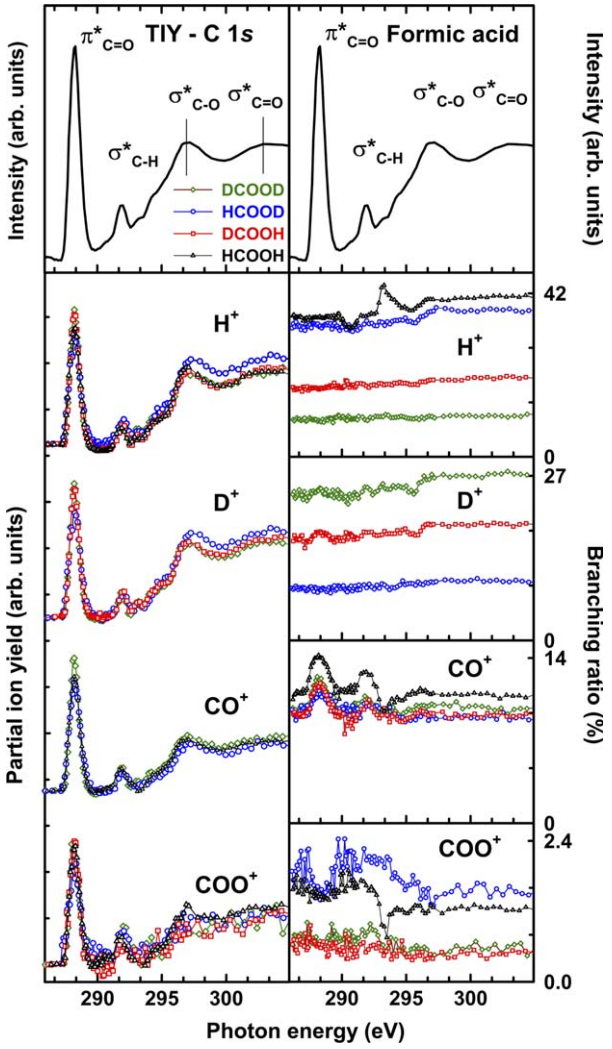

Fig. 6. C 1s partial ion yield and the photoion branching ratio spectra between 280 and 320 eV for H^+, D^+, CO^+, and COO^+ for all isotopes of formic acid, acquired in *focus* mode. The top panels are the TIY spectrum for comparison.

distorted by contamination with the OH counterpart via exchange with water on the walls of the inlet system. This has been taken into account in the analysis as far as possible.

The time-of-flight (TOF) apparatus has been described earlier [5,13]. Briefly, it consists of a McLaren type space charge focusing instrument [14] in which an electric field of 1050 V/cm (±1000 V over 19 mm) was applied to extract the photoelectrons and the parent and fragment ions into opposing electron and ion detection channels. An additional lens [15,16] was installed between the drift tube (DT) and the ion extraction grid. When operated in '*focus*' mode ($V_{\text{lens}} = -800$ V for $V_{\text{DT}} = -3800$ V) this lens focuses all fragment ions with kinetic energy less than 20 eV onto a microchannel plate (MCP) detector, regardless of their initial direction within a small ionization volume [13]. The lens can also be operated in two other modes, '*defocus*' ($V_{\text{lens}} = -3000$ V for $V_{\text{DT}} = -3800$ V), in which maximum sensitivity to angular and kinetic energy release distributions is achieved, and '*maximum*' ion mode ($V_{\text{lens}} = -2100$ V for $V_{\text{DT}} = -3800$ V) where the ion signal is strongest since it integrates over a larger volume, but there is residual kinetic energy and angular discrimination [13]. In this work we present results acquired in all three modes.

The ionization efficiency is the number of ions produced per absorbed photon. This was estimated by comparing the total ion yield spectrum (TIY) with that from photoabsorption, taken from the converted inner shell electron energy loss spectrum (ISEELS) of formic acid [26,30]. The branching ratio is defined as the ratio of the yield of a specific ion or ion pair to the total ion yield. The branching ratio spectra for each ion and ion pair were derived from the peak areas in PEPICO and PEPIPICO spectra measured at a series of energies, with high extraction fields and the *maximum* mode of the lens. After subtraction of the background of accidental coincidences, the first stop and second stop PEPICO signals were summed to generate the inputs to the branching ratio calculation. The quantitative partial ion yield (PIY) spectra were then derived by taking the product of the branching ratio and the absolute total ion yield (TIY) signal. The partial ion pair yield signals were derived by multiplying the TIY signal by the spectra for the branching ratio for each ion pair production derived by integrating peaks in the PEPIPICO signals.

Table 4
Branching ratios of single ions for corresponding ionic decay channels in isotopic formic acids (Focus Mode)

Branching ratios – Single ions								
Decay channel	val^{-1}				π^* (288.2 eV)			
	HCOOH	HCOOD	DCOOH	DCOOD	HCOOH	HCOOD	DCOOH	DCOOD
H^+	50.3	35.9	17.7	14.0	50.0	36.5	17.2	13.3
D^+	–	5.9	18.8	20.3	–	6.1	20.0	22.2
C^+	7.3	6.3	5.1	4.9	7.6	8.2	6.8	7.0
O^+	15.6	14.9	13.3	14.1	15.2	14.6	14.7	14.4
CO^+	8.6	9.6	9.1	9.3	10.1	10.9	10.9	10.7
COH^+	7.1	7.8	2.4	1.9	6.5	7.0	2.2	1.8
COD^+	–	5.9	17.7	16.7	–	4.7	13.7	14.0
Others	11.1	13.7	15.9	18.8	10.6	12.0	14.5	16.7
	σ^*(C–H) (292.0 eV)				C 1s^{-1} (296.1 eV)			
	HCOOH	HCOOD	DCOOH	DCOOD	HCOOH	HCOOD	DCOOH	DCOOD
H^+	52.5	36.7	18.8	13.3	52.9	38.2	19.0	14.2
D^+	–	6.9	19.3	22.6	–	7.1	20.1	23.4
C^+	8.9	7.1	6.0	6.4	7.2	8.2	6.3	6.6
O^+	17.8	15.7	14.8	14.2	17.9	16.6	16.2	16.3
CO^+	9.2	10.5	9.7	9.2	8.5	9.2	9.0	8.9
COH^+	4.4	6.0	2.3	1.4	4.9	5.1	2.2	1.6
COD^+	–	5.8	15.8	15.8	–	5.4	13.4	14.3
Others	7.1	11.4	13.2	17.2	8.7	10.1	13.7	14.8

	Continuum (320 eV)			
	HCOOH	HCOOD	DCOOH	DCOOD
H^+	55.5	40.1	20.7	14.7
D^+	–	7.7	21.2	25.3
C^+	8.2	8.2	6.6	6.8
O^+	17.8	17.3	16.8	17.0
CO^+	7.7	8.3	8.5	8.2
COH^+	3.6	4.3	1.8	1,5
COD^+	–	4.5	11.9	12.4
Others	7.2	9.6	12.5	14.1

3. Results and discussion

3.1. Total ion yield and ionization efficiency

Fig. 1 presents the TIY spectrum of formic acid, which is the average of data for HCCOH and DCOOD. There were no detectable differences among the TIY spectra of the four isotopic species. This TIY spectrum is at lower resolution, but otherwise similar to the inner shell excitation spectrum as recorded by electron energy loss [26]. The energies and assignments of the spectral features are listed in Table 1. The assignments have been discussed in detail elsewhere [26]. Briefly, the intense low energy peak at 288.2 eV arises from the C 1s $\rightarrow \pi^*_{C=O}$ transition, that at 291.8 eV is the C 1s $\rightarrow \sigma^*_{CH}$ transition of particular interest in this work, the shoulder at 294.2 eV is unresolved Rydberg states leading to the C 1s ionization continuum, and the 2 peaks in the ionization continuum at 297 and 303 eV are the σ^*_{C-O} and $\sigma^*_{C=O}$ resonances, respectively. Fig. 1 also plots the photoabsorption spectrum of formic acid taken from the literature [26,30]. The as-measured ISEELS spectrum [30] was re-processed to include the pre-edge signal on an absolute oscillator strength scale. The intensity of the TIY signal was set to an absolute oscillator strength scale by requiring the ionization efficiency (η) between 310 and 320 eV to be have a value of 2. With this scaling the value of η below the onset of core excitation is 1.2(1), with the excess above 1 related to direct dissociative ionization. The value of η is reduced in the region of both 1s $\rightarrow \pi^*$ and 1s $\rightarrow$ Rydberg excitations, and then approaches 2 above the C 1s ionization potential (IP) [31], although there is a region of reduced η between 296 and 308 eV, probably due to post-collision interaction. There also appears to be some further increase in the value of η above 325 eV, which could be due to shake-off processes leading to dissociative triple ionization.

3.2. PEPICO and PIPICO signals

Fig. 2 presents the PEPICO time-of-flight mass spectrometry signals for HCOOH, HCOOD, DCOOH and DCOOD, acquired in *maximum* ion mode at 250 eV (below C 1s onset and O 1s second order) and 307 eV (maximum of C 1s $\rightarrow \sigma^*_{C=O}$ resonance). The H^+ or D^+ ion (depending on the isotope) is the strongest peak in these spectra at each energy, although its contribution is relatively greater at 307 eV due to the higher extent of fragmentation following inner-shell ionization. Four other groups of ions can also be distinguished. They are A_xC^+ (C^+, HC^+, DC^+), A_xCO^+ (CO^+, HCO^+, DCO^+), OA_x^+ (O^+, OH^+, OH_2^+, OD^+) and the A_xCOO^+ group (COO^+, $HCOO^+$, $DCOO^+$), where A = H or D and $x = 0$, 1. We note that significant H^+ signal is observed in the mass spectrum of DCOOD, whereas none would be expected. Two effects could be the source of that signal: the limited isotopic purity at the hydroxy position (~90%) and H/D exchange with water coating the walls of the gas inlet system. The very large H^+ signal in the mass spectrum of HCOOD may also be affected in the same way. In future experiments of this type, the gas inlet system should be completely saturated with D_2O prior to introducing a sample deuterated at an exchangeable site.

Table 2 lists the assignments for the PEPICO signals derived by converting the measured flight times to mass-to-charge ratio (m/e). PEPICO mass spectra were measured at many different photon energies between 120 and 307 eV. Fig. 3 shows the PEPICO signals for HCOOH, acquired in *maximum* ion mode at 120, 250, 280, 290, 294, and 307 eV. Although a significant increase in fragmentation is observed as the energy is increased, particularly when going from below to above the C 1s ionization onset, overall the fragmentation pattern remains similar at all photon energies.

Fig. 4 shows the photoion–photoion-coincidence (PIPICO) signal for HCOOH, HCOOD, DCOOH and DCOOD, acquired in *maximum* ion mode at 250 eV and

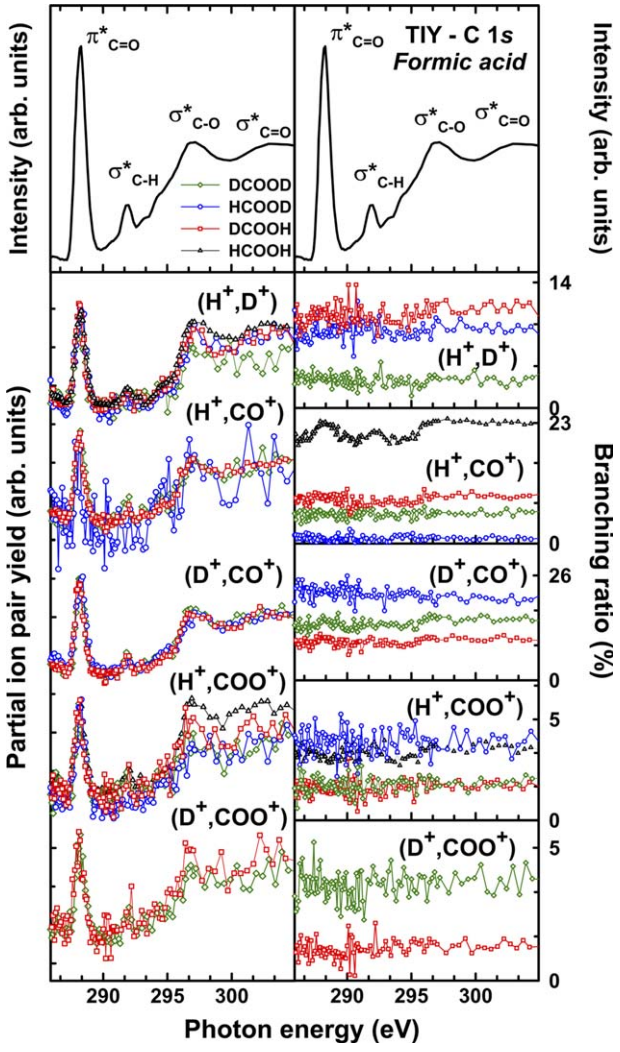

Fig. 7. Branching ion pair ratios (BIPR) and partial ion pair yield (PIPY) spectra for several ion pairs in the C 1s region in *maximum* ion mode, derived from PIPICO data.

at 307 eV. In PIPICO, only the time differences between correlated ion pairs are measured, giving rise to ambiguities in the identification of the participating ions. However the major features can be identified by a careful comparison of the predicted and observed flight time differences. In addition the assignments were verified by comparison to the photoelectron–photoion–photoion-coincidence (PEPIPICO) results, in which the peak assignments are totally unambiguous (see below). Table 3 presents assignments for the PIPICO signals based on the flight time differences (Δt) for the component ions. Fig. 5 shows the PIPICO signals for HCOOH, acquired in *maximum* ion mode at 120, 250, 280, 290, 294 and 307 eV. As with the singles PEPICO signals, the changes with increasing photon energy are relatively minor.

3.3. Branching ratio (BR) and partial ion yield (PIY) spectra

Fig. 6 presents the photoion branching ratios and the associated partial ion yield spectra between 280 and 320 eV acquired in *focus* mode for the production of H^+, D^+, CO^+, and COO^+ ions, which are the major ions generated by soft X-ray ionization of the four isotopes of formic acid. The C 1s total ion yield (TIY) spectrum is also plotted in the top panel to facilitate identification of possible state specific fragmentation. Aside from small changes in the shapes of the D^+ and H^+ yield spectra at 297 eV (σ^*_{C-O}) and in the shapes of the CO^+ and COO^+ yield spectra at 291.8 eV (σ^*_{C-H}), the results are similar for all isotopic forms. Relative to the TIY spectrum, the singles yields of the H^+, D^+ and COO^+ ions are suppressed at 288.2 eV ($\pi^*_{C=O}$) and at 291.8 eV (σ^*_{C-H}), but the singles CO^+ yield is enhanced at 292 eV (σ^*_{C-H}).

Table 4 presents branching ratios at selected energies derived from the quantitative *focus* mode results. As seen in Fig. 6, there is relatively little change in branching ratio throughout the C 1s region. The largest changes are between the pre-C 1s-onset and the C 1s continuum, in the CO^+ and COO^+ yields, which is associated with the greater extent of ionic fragmentation following production of the C 1s core hole.

Table 5
Branching ratios of ion pairs for corresponding ionic decay channels in isotopic formic acids (Focus Mode)

Branching ratios – Ion pairs								
Decay channel	val^{-1}				π^* (288.2 eV)			
	HCOOH	HCOOD	DCOOH	DCOOD	HCOOH	HCOOD	DCOOH	DCOOD
(H^+,D^+)	–	10.6	12.3	10.3	–	10.9	11.7	6.4
(H^+,C^+)	18.0	18.5	2.6	5.3	23.9	18.1	4.4	4.0
(H^+,O^+)	48.1	37.0	12.1	13.4	40.6	34.7	12.9	12.4
(H^+,CO^+)	18.0	16.1	5.9	4.9	22.1	19.5	6.4	5.0
(C^+,O^+)	7.2	1.4	5.0	3.3	5.2	3.1	4.5	2.8
(D^+,C^+)	–	NC	NC	5.3	–	NC	NC	10.7
(D^+,O^+)	–	8.1	11.1	22.7	–	6.6	10.9	20.1
(D^+,CO^+)	–	NC	3.6	6.9	–	NC	7.1	7.2
Others	8.7	8.3	47.4	27.9	8.2	7.1	42.1	31.4
	σ^*(C–H) (292.0 eV)				C 1s^{-1} (296.1 eV)			
	HCOOH	HCOOD	DCOOH	DCOOD	HCOOH	HCOOD	DCOOH	DCOOD
(H^+,D^+)	–	11.3	10.8	9.3	–	10.9	11.6	9.2
(H^+,C^+)	23.2	18.5	5.7	4.4	21.4	18.5	4.7	2.8
(H^+,O^+)	45.2	40.1	12.3	10.1	45.5	36.9	14.2	11.5
(H^+,CO^+)	18.4	14.8	5.0	4.7	22.1	19.0	5.6	5.5
(C^+,O^+)	7.2	5.0	2.9	2.6	4.5	2.1	4.3	2.7
(D^+,C^+)	–	NC	NC	9.3	–	NC	NC	6.2
(D^+,O^+)	–	5.3	11.2	18.9	–	6.6	11.6	20.9
(D^+,CO^+)	–	NC	6.0	5.8	–	NC	6.5	8.2
Others	6.0	5.0	46.1	34.9	6.5	6.0	41.5	33.0
	Continuum (320 eV)							
	HCOOH		HCOOD		DCOOH		DCOOD	
(H^+,D^+)	–		11.1		12.7		9.7	
(H^+,C^+)	23.4		19.3		4.7		4.0	
(H^+,O^+)	44.9		34.9		14.3		11.6	
(H^+,CO^+)	18.9		19.2		6.3		4.4	
(C^+,O^+)	6.2		3.2		5.2		4.8	
(D^+,C^+)	–		NC		NC		11.3	
(D^+,O^+)	–		7.3		12.2		22.5	
(D^+,CO^+)	–		NC		6.3		6.5	
Others	6.6		5.0		38.3		25.2	

3.4. Partial ion pair yield (PIPY) and branching ion pair ratio (BIPR) spectra

Fig. 7 plots the branching ratios for ion pair production and the partial ion pair yield spectra for several ion pairs in the C 1s region, derived from PIPICO data measured in *maximum* ion mode. The branching ratios summed over groups of ions as identified earlier (A_xC^+ (C^+, HC^+, DC^+), A_xCO^+ (CO^+, HCO^+, DCO^+), OA_x^+ (O^+, OH^+, OH_2^+, OD^+) and the A_xCOO^+) are summarized in Table 5. Aside from small changes in D^+ and H^+ ion line shapes at 297 eV (σ^*_{C-O}) and CO^+ and COO^+ ion yield line shapes at 292 eV (σ^*_{C-H}) the results are similar for all isotopic forms.

3.5. PEPIPICO

The photoelectron–photoion–photoion coincidence (PEPIPICO) spectra of the four formic acid isotopes measured at 305 eV (near the C 1s → σ* resonance maximum) with the lens operated in *defocus* mode are presented in Fig. 8. The relative ion pair yields in the PEPIPICO signals

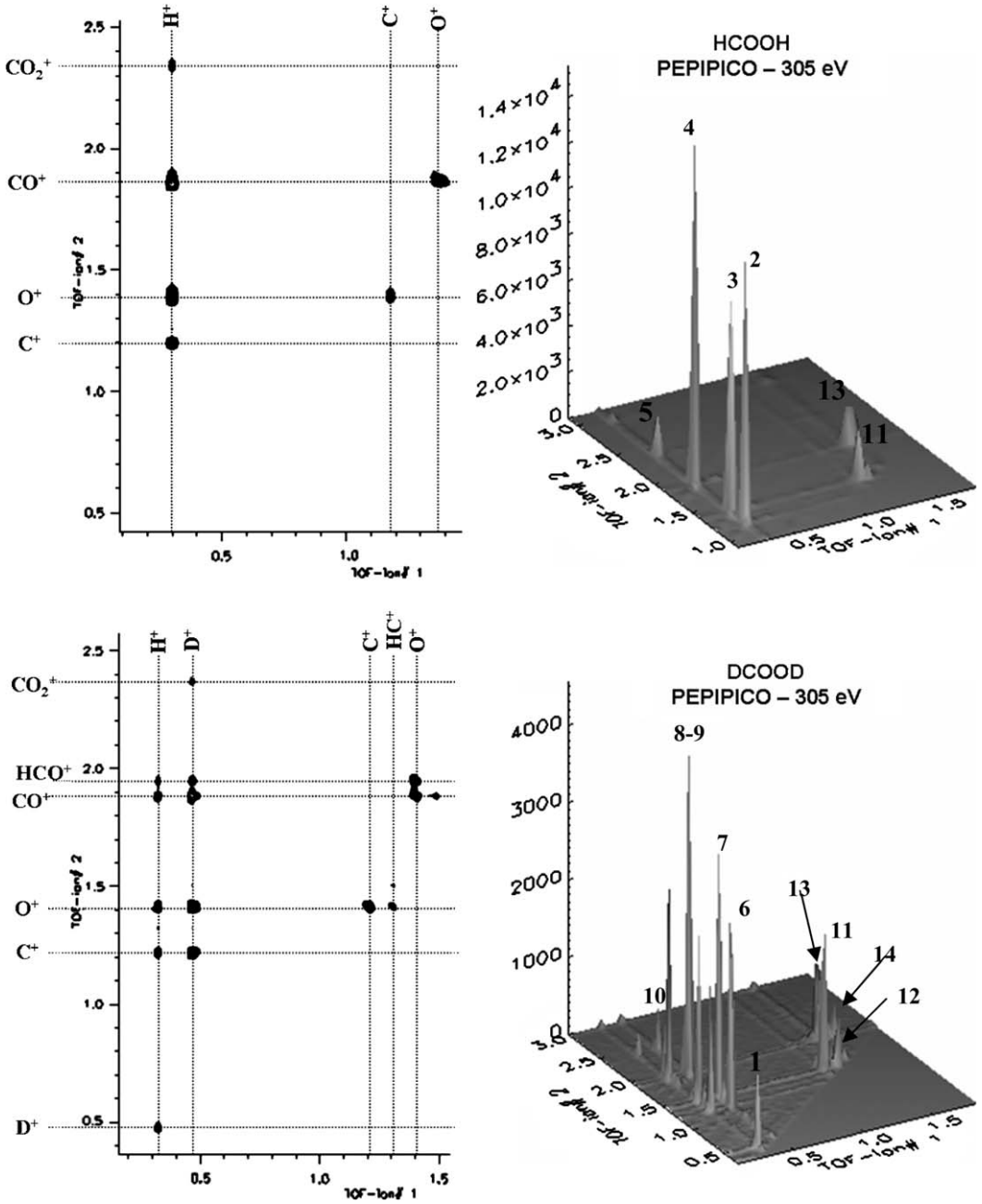

Fig. 8. Photoelectron–photoion–photoion coincidence (PEPIPICO) spectra measured at 305 eV with the lens operated in *defocus* mode. The assignments are: 1 – (H^+,D^+); 2 – (H^+,C^+); 3 – (H^+,O^+); 4 – (H^+,CO^+); 5 – (H^+,COO^+); 6 – (D^+,C^+); 7 – (D^+,O^+); 8 – (D^+,CO^+); 9 – (D^+,COO^+); 10 – (C^+,O^+); 11 – (O^+,CO^+).

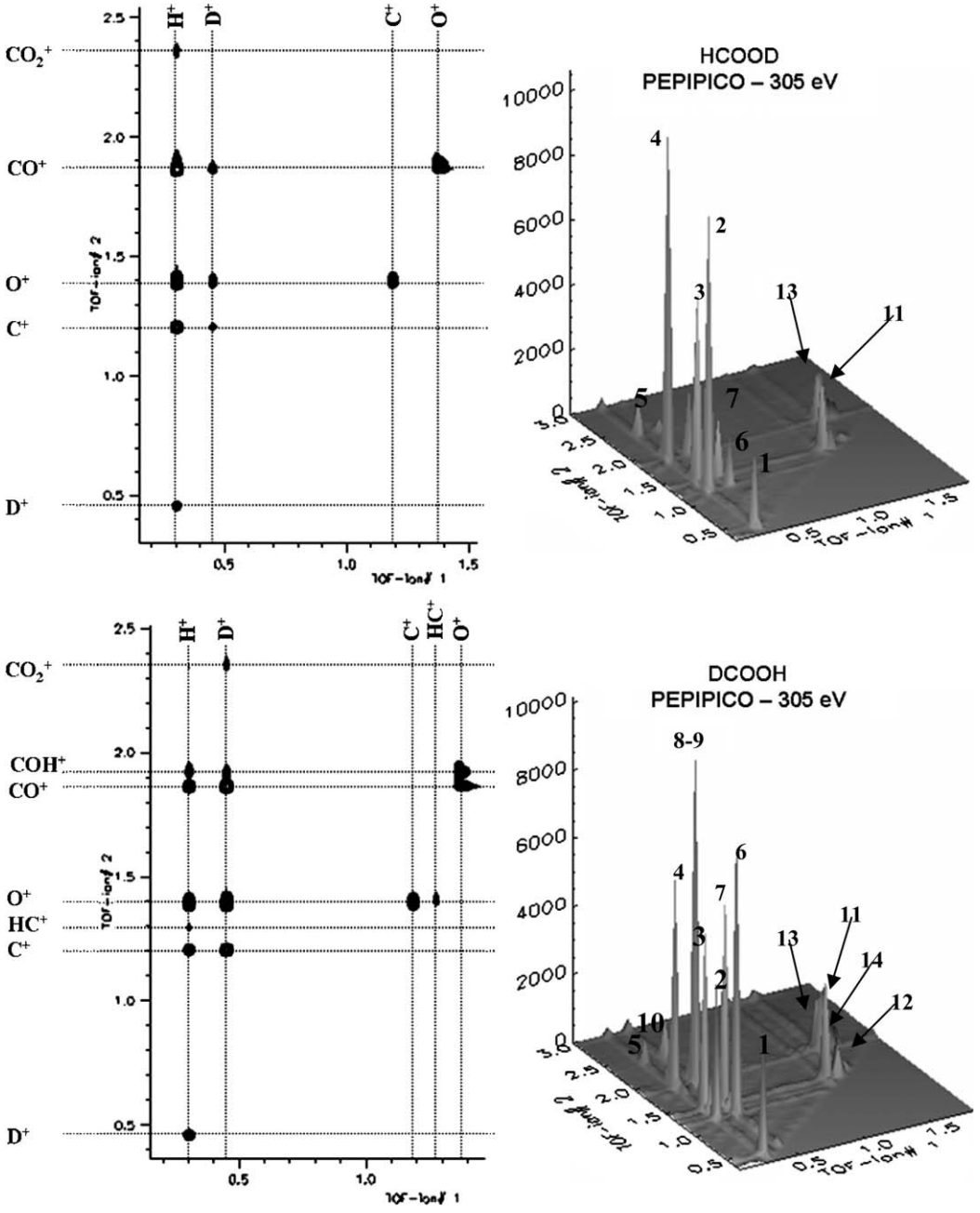

Fig. 8 (*continued*)

recorded in *maximum* ion mode were very similar, but the *defocus* mode results are shown as they are of higher statistical precision. They illustrate clearly the advantage of PEPIPICO relative to PIPICO. In particular each ion of the pair is explicitly defined by its flight time. Table 6 presents assignments for the PEPIPICO signals based on the flight time differences (Δt) for the component ions.

3.6. Comparison of gas phase partial ion yields with formate/Si(100) PSID yields

Fig. 9 shows the photon stimulated ion desorption (PSID) yield curves of D^+, CDO^+, O^+, and CD^+ from DCOO/Si(100) in the C 1s excitation region, along with the Auger electron yield (AEY) curve, taken from Ref. [3]. A strong enhancement of D^+ is observed at the σ^*_{C-D} transition (292 eV), which was the motivation for this gas phase study. Fig. 9 also shows the D^+ ion yield spectrum from DCOOH and the spectra for producing all ion pairs from DCOOH which involve D^+ – those in coincidence with C^+, O^+, CO^+, COH^+ and CO_2^+. If the D^+ enhanced yield seen in the X-ray stimulated desorption of deuteroformate from Si(001) was a significant component of the ionic fragmentation of the ($C\ 1s^{-1}$, σ^*_{C-H}) state at 291.8 eV, then these are the possible channels which might exhibit the gas phase counterpart signal. As Fig. 9 shows,

Table 6
Assignments for PEPIPICO signals based on their difference flight time (Δt)

#	Coincidence (μs)	Ion pair
1	[0.35,0.50]	(H^+,D^+)
2	[0.35,1.25]	(H^+,C^+)
3	[0.35,1.44]	(H^+,O^+)
4	[0.35,1.91]	(H^+,CO^+)
5	[0.35,2.41]	(H^+,COO^+)
6	[0.50,1.25]	(D^+,C^+)
7	[0.50,1.44]	(D^+,O^+)
8	[0.50,1.91]	(D^+,CO^+)
9	[0.50,1.95]	(D^+,HCO^+)
10	[0.50,2.41]	(D^+,COO^+)
11	[1.25,1.44]	(C^+,O^+)
12	[1.30,1.44]	(HC^+,O^+)
13	[1.44,1.91]	(O^+,CO^+)
14	[1.44,1.95]	(O^+,HCO^+)

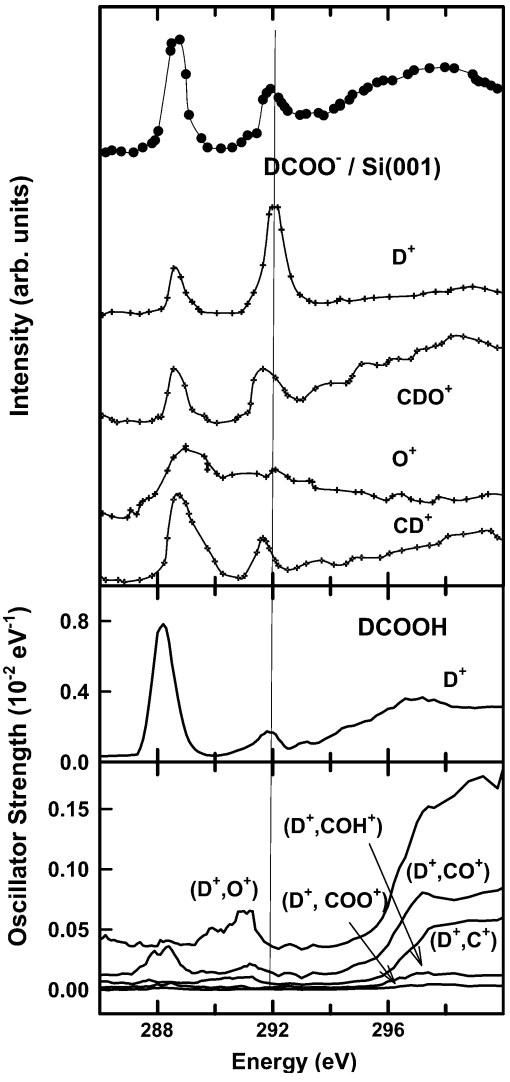

Fig. 9. (upper) Auger electron yield (AEY) and ion desorption yields from $DCOO^-$/Si(100) (taken from ref. 3). (middle) partial D^+ ion yield, and (lower) partial (D^+, CO^+) and [(D^+,C^+) (D^+, O^+), (D^+,COO^+), (D^+,COH^+)] ion pair yields for C 1s excitation of gaseous DCOOH, acquired in *focus* mode.

none of these channels in the gas phase ionic fragmentation have significant enhancements at 291.8 eV. Only the (D^+, O^+) channel has a small peak, but it is ~0.5 eV below the position of the σ^*_{C-H} resonance. This suggests that the mechanism for producing D^+ from PSID of DCOO/Si(100) is either an extremely minor channel which we have not been able to detect in the gas phase, or alternatively, it arises from an ultrafast dissociation involving C–H or C–D bond breaking and thus initial formation of neutral H and D. If so, the channel leading to the observed enhanced D^+ yield in the ionic desorption must involve a specific long-range process in which the electron on the departing D atom is involved in the autoionization of the core hole [4,5]. This channel is detected only because most other ionic species (in particular, other channels leading to D^+) are neutralized by electron transfer from the surface. The ultrafast decay producing D^+ is likely to be relatively more visible in surface PSID due to suppression of other channels by re-neutralization of ions produced in Auger decay while the core excited species is still attached to the surface.

Fig. 9 also shows that the Auger electron yield (AEY) spectrum of adsorbed formate is different from the TIY spectrum of gas phase formic acid in two respects. The $\pi^*_{C=O}$ and σ_{C-O} resonances are at slightly different energies, which is consistent with the modified bonding and geometry. Specifically, formate has two equal C–O bonds and thus only a single σ^*_{C-O} continuum resonance whereas formic acid has two distinct C–O bonds so there are distinct σ^*_{C-O} and $\sigma^*_{C=O}$ resonances in the gas phase spectrum. Second, the surface AEY spectrum has considerably enhanced σ^*_{C-O} and σ^*_{C-H} intensities, and suppressed $\pi^*_{C=O}$ intensity relative to the gas phase formic acid spectrum. This indicates there is a polarization effect in the surface PSID data, with the in-plane σ^* resonances enhanced relative to the π^* resonance, on account of the highly aligned geometry of the formate molecule perpendicular to the surface. The NEXAFS signals have been interpreted to indicate a geometry with the molecular plane of the adsorbed formate group is tilted away from surface normal by an average angle of $21 \pm 2°$ [32]. This geometry has been confirmed by ab initio calculations [33].

4. Summary

Multi-ion coincidence (PEPICO, PIPICO, PEPIPICO) and partial ion and ion-pair yield spectra for all ions of gaseous formic acid in all four isotopically substituted forms have been measured at the C 1s edge. Aside from small changes in D^+ and H^+ ion line shapes at 297 eV (σ^*_{C-O}) and CO^+ and COO^+ ion yield line shapes at 291.8 eV (σ^*_{C-H}) the results are similar for all isotopic forms. In the gas phase, the H^+, D^+, COO^+ single ion yields are suppressed at 288.2 eV (π^* C=O) and at 291.8 eV (σ^* C–H), but the singles CO^+ yield and the (X^+, COO^+) pair yields (X = H or D) are enhanced at 291.8 eV (σ^* C–H) In formate (DCOO) adsorbed on Si(100), a strong enhancement of D^+ was observed at

291.8 eV, but there is no direct counterpart to this in the gas phase. The enhanced D^+ yield in PSID from surface adsorbed $DCOO^-$/Si(100) may arise from an ultrafast decay involving neutral D^* which is ionized at a distance from the residual core excited fragment. It becomes visible in the surface PSID due to re-neutralization of other ions produced in Auger decay while the core excited species is still attached to the surface.

Acknowledgement

Measurements at the Mark II grasshopper of the Synchrotron Radiation Centre, funded by NSF (Award No. DMR-0084402). Research supported by NSERC (Canada), the Canada Research Chair program, FAPERJ (Brazil) and CAPES (Brazil). Antonio Guerra gratefully acknowledges a CAPES (Brazil) graduate fellowship. We acknowledge assistance of the staff scientists of the Canadian Synchrotron Radiation Facility, which is supported by an NSERC MFA grant.

References

[1] Y. Huang, H.G. Huang, K.Y. Lin, Q.P. Liu, Y.M. Sun, G.Q. Xu, Surf. Sci. 549 (2004) 255.
[2] D.A. Outka, J. Stöhr, R.J. Madix, H.H. Rotermund, B. Hermsmeier, J. Solomon, Surf. Sci. 185 (1987) 53.
[3] H. Ikeura-Sekiguchi, T. Sekiguchi, K. Tanaka, Phys. Rev. B 53 (1996) 12655.
[4] P. Morin, I. Nenner, Phys. Rev. Lett. 56 (1986) 1913.
[5] A.P. Hitchcock, J.J. Neville, in: T.K. Sham (Ed.), Chemical Applications of Synchrotron Radiation, World Scientific, 2001 and references therein.
[6] D. Menzel, R. Gomer, J. Chem. Phys. 40 (1964) 1164.
[7] W. Wurth, C. Schneider, R. Treichler, E. Umbach, D. Menzel, Phys. Rev. B 35 (1987) 7741.
[8] T.E. Madey, Science 234 (1986) 316.
[9] P. Avouris, R.E. Walkup, Ann. Rev. Phys. Chem 40 (1989) 173.
[10] R.C. Bilodeau, G.D. Ackerman, A. Aguilar, J.D. Bozek, G. Turri, N. Berrah, in: XXIII International Conference on Photonic, Electronic, and Atomic Collisions (ICPEAC), Stockholm, Sweden, July 2003.
[11] I. Nenner, P. Morin, in: U. Becker, D.A. Shirley (Eds.), VUV and Soft X-Ray Photoionization, Plenum Press, New York, 1996, p. 291.
[12] A.P. Hitchcock, J.J. Neville, A. Jürgensen, R.G. Cavell, J. Electron Spectrosc. Relat. Phenom. 88–91 (1998) 71.
[13] A.C.O. Guerra, J.B. Maciel, C.C. Turci, R.C. Bilodeau, A.P. Hitchcock, Can. J. Chem. 82 (2004) 1052.
[14] W.C. Wiley, H. McLaren, Rev. Sci. Instrum. 26 (1955) 1150.
[15] J.B. Maciel, E. Morikawa, G.G.B. de Souza, in: Presented at the 10th US National Conference on Synchrotron Radiation Instrumentation, Ithaca, New York, 1997.
[16] A.C.F. Santos, C.A. Lucas, G.G.B. de Souza, Chem. Phys. 282 (2002) 315.
[17] J. Stöhr, J.L. Gland, W. Eberhardt, D. Outka, R.J. Madix, F. Sette, R.J. Koestner, U. Doebler, Phys. Rev. Lett. 51 (1983) 2414.
[18] G. Thornton, S. Crook, Z. Chang, Surf. Sci. 415 (1998) 122.
[19] Z. Chang, G. Thornton, Surf. Sci. 459 (2000) 303.
[20] Z. Chang, G. Thornton, S. Crook, Surf. Sci. 462 (2000) 68.
[21] H. Ikeura-Sekiguchi, T. Sekiguchi, Surf. Sci. 390 (1997) 214.
[22] T. Sekiguchi, H. Ikeura-Sekiguchi, K. Tanaka, Surf. Sci. 390 (1997) 199.
[23] H. Ikeura-Sekiguchi, T. Sekiguchi, Surf. Sci. 433–435 (1999) 549.
[24] T. Sekiguchi, H. Ikeura-Sekiguchi, M. Imamura, N. Matsubayashi, H. Shimada, Y. Baba, Surf. Sci. 482–485 (2001) 279.
[25] H. Ikeura-Sekiguchi, T. Sekiguchi, N. Saito, I.H. Suzuki, J. Synchrotron Rad. 8 (2001) 548.
[26] I. Ishii, A.P. Hitchcock, J. Chem. Phys. 87 (1987) 830.
[27] B. Ruscic, M. Schwarz, J. Berkowitz, J. Chem. Phys. 91 (1989) 6780.
[28] A. Mocellin, R.R.T. Marinho, L.H. Coutinho, F. Burmeister, K. Wiesner, A. Naves de Brito, Chem. Phys. 289 (2003) 163.
[29] H.M. Boechat-Roberty, S. Pilling, A.C.F. Santos, Astron. Astrophys. 438 (2005) 915.
[30] A.P. Hitchcock, D. Mancini, J. Electron Spectrosc. Rel. Phenom. 67 (1994) 1, and updates, available from http://unicorn.mcmaster.ca .
[31] W.L. Jolly, K.D. Bomben, C.J. Eyermann, At. Data Nucl. Data Tables 31 (1984) 433.
[32] M. Carbone, M.N. Piancastelli, M.P. Casaletto, R. Zanoni, G. Comtet, G. Dujardin, L. Hellner, Chem. Phys. 289 (2003) 93.
[33] X. Lu, Q. Zhang, M.C. Lin, Phys. Chem. Chem. Phys. 3 (2001) 2156.